Eur. Phys. J. A (2018) **54**: 142
DOI 10.1140/epja/i2018-12575-5

THE EUROPEAN PHYSICAL JOURNAL A

Special Article – New Tools and Techniques

Development of a two-stage detection array for low-energy light charged particles in nuclear astrophysics applications

M. Romoli[1,a], L. Morales-Gallegos[2,3,1], M. Aliotta[2], C.G. Bruno[2], R. Buompane[3,1], A. D'Onofrio[3,1], T. Davinson[2], M. De Cesare[4,1], A. Di Leva[5,1], P. Di Meo[1], J. Duarte[3,1], L. Gasques[6,3,1], L. Gialanella[3,1], G. Imbriani[5,1], G. Porzio[3,1], D. Rapagnani[3,7,8], and A. Vanzanella[1]

[1] INFN, Sezione di Napoli, Complesso Universitario MSA, via Cintia snc, I-80126 Napoli, Italy
[2] SUPA, School of Physics and Astronomy, University of Edinburgh, Edinburgh, UK
[3] Dipartimento di Matematica e Fisica, Università della Campania "L. Vanvitelli", Caserta, Italy
[4] Department of Diagnostic Methodologies and Measurement Techniques, Italian Aerospace Research Centre (CIRA), Capua (CE), Italy
[5] Dipartimento di Fisica, Università di Napoli "Federico II", Napoli, Italy
[6] Departamento de Fisica Nuclear, Instituto de Fisica da Universidade de São Paolo, São Paolo, Brazil
[7] Dipartimento di Fisica e Geologia, Università degli Studi di Perugia, Perugia, Italy
[8] INFN, Sezione di Perugia, Perugia, Italy

Received: 6 March 2018 / Revised: 15 June 2018
Published online: 30 August 2018

Communicated by A. Di Pietro

Abstract. A new detection array called GASTLY (GAs-Silicon Two-Layer sYstem) has been designed to detect and identify low-energy light particles emitted in nuclear reactions of astrophysical interest. Devoted to the measurement of nanobarn cross-sections, the system is optimised for large solid angle coverage and for low-energy detection thresholds. The array consists of eight modules, each comprising an ionisation chamber and a large area silicon strip detector. Its modularity and versatility allow for use in a variety of experiments. Here we report on the performance of the array as obtained during its commissioning phase with standard α-particle sources and during in-beam tests with an intense ^{12}C beam. Typical energy resolutions $\Delta E(\mathrm{FWHM})/E$ of about 3% and 2% were obtained for the ionisation chambers and the silicon detectors, respectively. The status of the development of individual strip readout, based on ASIC technology, is also presented.

1 Motivation

Nuclear reactions of astrophysical interest between stable nuclei normally take place at thermal (*i.e.*, sub-Coulomb) energies in stars and are characterised by reaction cross sections in the nanobarn to picobarn range or lower [1, 2]. When studying such reactions in terrestrial laboratories, the corresponding low yields translate into the need for high beam currents (μA to mA), prolonged run times, high detection efficiency and large solid angle coverage. In addition, low interaction energies typically imply low-energy reaction products, essentially dominated by the reaction Q-value, which poses further challenges to their detection and identification. A further complication arises from beam-induced background, namely the occurrence of reactions other than the one of interest (for example, on impurities in the target), but whose cross sections are significantly higher than the one under study. Special effort must then be devoted to produce high-purity targets and to minimise any beam interaction with other components of the setup, such as apertures and collimators [1,2]. The presence of any beam-induced background also clearly adds the need to identify reaction channels for proper background subtraction, through the use of standard techniques, such as ΔE-E particle identification, time of flight, or mass separators [3,4].

An extensive campaign of measurements was recently undertaken at the Centre for Isotopic Research on the Cultural and Environmental heritage (CIRCE) of the Università della Campania "L. Vanvitelli" (Caserta, Italy) for the study of one of the most important reactions in nuclear astrophysics, namely the fusion of two ^{12}C nuclei known as carbon burning. Carbon burning represents a key stage in the evolution of massive stars ($M > 8\,M_{\odot}$) as it determines whether these will wither away as white dwarfs or end up in catastrophic explosions known as supernovae (see, for example, [5] and references therein). At characteristic temperatures of 0.3–1.9 GK, corresponding

[a] e-mail: romoli@na.infn.it (corresponding author)

to interaction energies $E_{\rm cm}$ = 1.0–3.5 MeV, carbon fusion proceeds through two main channels: ^{12}C(^{12}C, p)^{23}Na (Q-value = 2.24 MeV) and ^{12}C(^{12}C, α)^{20}Ne (Q-value = 4.62 MeV). A number of excited states in the residual nuclei can be populated, leading to ejected proton and α-particle energies up to a few MeV, depending on beam energy and detection angle.

Despite decades of experimental efforts devoted to the measurement of these important reactions using both γ-ray [6–13] and particle [14–17] spectroscopy, the energy region of astrophysical interest has barely been reached and further investigations are needed to achieve better extrapolations of the astrophysical $S(E)$ factor.

Results from cross section measurements of carbon fusion reactions performed at CIRCE will be presented in forthcoming papers. Here, we report on the development of the modular detector array GASTLY (GAs-Silicon Two-Layer sYstem) used for such measurements. The array consists of a two-stage detection system based on ionisation chambers and large area silicon strip detectors and has been specifically designed to meet the requirements of low-energy ion detection for nuclear astrophysics studies, namely large solid angle coverage, as well as high angular- and energy resolution. After a brief description of the detector design, we report the results of tests performed with beam and with standard α-particle sources.

2 Experimental setup

For the purpose of the carbon fusion reaction studies, it was necessary: a) to use thick ($\simeq$ 1 mm) and water-cooled targets (to control the target temperature during intense carbon-beam bombardment), and b) to avoid exposing the detectors to the high flux of scattered beam particles. For these reasons, the detection of reaction products (protons and alpha particles up to a few MeV) was performed at backward angles. In order to cover as large a solid angle as possible, using only a limited number of (expensive) silicon strip detectors, the GASTLY detector array was designed so as to allow for up to eight individual modules to be arranged around the beam axis in the backward hemisphere. However, thanks to its modularity and flexible configuration, the GASTLY array can be used also in experiments where angular distribution measurements at forward angles and with thin targets are required.

Each module consists of an ionisation chamber for the ΔE stage and a large area (about $6 \times 6\,{\rm cm}^2$) silicon strip detector for the E stage, placed immediately behind the IC (see sects. 3.1 and 3.2). Figure 1 shows a schematic 3D view of the full GASTLY array. Individual module positions, angular ranges, and distances to target are given in table 1. In the configuration used for the carbon fusion measurements (hereafter the ^{12}C experiment), only four of the possible eight modules were used, at nominal positions 3 (122.5°), 5 (144.5°), 7 (156.5° UP), and 8 (156.5° DOWN).

The scattering chamber was maintained under vacuum at typical pressures of 10^{-6} mbar. The beam entered the scattering chamber passing through a copper beam pipe maintained at liquid nitrogen temperature to minimise carbon deposition on target. The target, consisting of either natural graphite (NG) or highly ordered pyrolytic graphite (HOPG), was mounted on a target holder which was water-cooled (at about 5 °C) and surrounded by a hemi-spherical electrode with square ports, larger than the detector entrance windows, to allow for the passage of particles to be detected. The electrode, not shown in fig. 1, was maintained at a negative potential (−300 V) for electron suppression. This is needed to correctly read the current (and thus integrate the charge) delivered on target. There is no background contribution arising from this set-up, as was verified in measurements with and without the sphere both with beam and with an α-particle source. A thermal imaging camera FLIR SC325 [18], mounted on a port of the scattering chamber, was used to continuously monitor the target temperature during beam

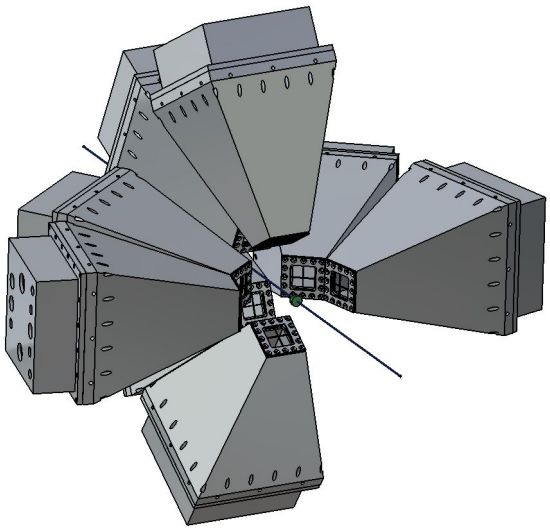

Fig. 1. GASTLY set-up with 8 modules positioned around the target in the backward hemisphere, with respect to the beam direction.

Table 1. Central angle θ_0 and angular coverage of all eight GASTLY detector modules, with opening angles ($\Delta\theta$) and distances ($d_{\rm TC}$) between target and front face (*i.e.*, cathode) of each ionisation chamber (see text for details).

Det. pos.	θ_0 (deg)	$\theta_{\rm min}$ (deg)	$\theta_{\rm max}$ (deg)	$\Delta\theta$ (deg)	ϕ_0 (deg)	$d_{\rm TC}$ (mm)
1	104.5	95.0	114.0	19.0	0	54
2	104.5	95.0	114.0	19.0	180	54
3	122.5	113.0	132.0	19.0	90	54
4	122.5	113.0	132.0	19.0	270	54
5	144.5	135.0	154.0	19.0	0	54
6	144.5	135.0	154.0	19.0	180	54
7	156.5	150.3	162.7	12.4	90	74
8	156.5	150.3	162.7	12.4	270	74

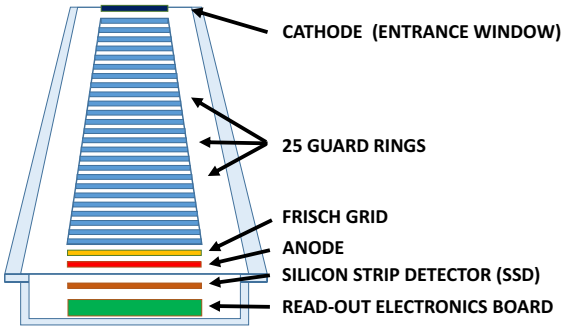

Fig. 2. Schematic cross-sectional view of a GASTLY module. Key components of the ionisation chamber are indicated. Both the ionisation chamber and the silicon strip detector are contained within an aluminium housing shaped as a truncated pyramidal structure with square section.

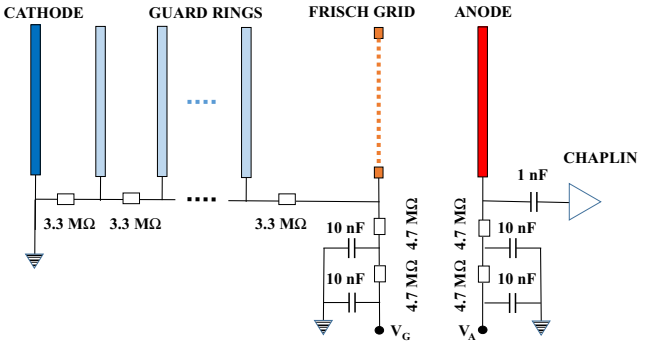

Fig. 3. Scheme of the bias and filtering circuit for the GASTLY ionisation chamber. The bias is applied to the Frisch grid and goes to ground potential at the cathode, through a chain of 3.3 MΩ resistors connected in series. This resistive partition of the potential is used to bias the guard rings.

bombardment. The scattering chamber was surrounded by a sealed plexiglass box which could be kept in an argon or nitrogen atmosphere to reduce residual hydrogen contamination in the chamber and hence on target. The rest gas in the chamber was monitored by a quadrupole mass spectrometer (Pfeiffer Prisma QME 200).

3 GASTLY detector description

Each GASTLY module consists of an ionisation chamber (IC) and a silicon strip detector (SSD), both housed in an aluminium pyramidal case, which provide the ΔE-E stages for standard particle identification. A detailed description of each detector is given in the following sections.

3.1 Ionisation chamber

The ionisation chamber consists of a fiberglass (FR-4) frame shaped as a truncated pyramid with square section. Its key components are a cathode (entrance window), a Frisch grid, an anode, several guard rings, and a suitable gas maintained at an appropriate pressure (depending on application). A schematic view of an individual GASTLY module is shown in fig. 2.

For the ^{12}C experiment, the entrance window was a $23.0 \times 23.0\,\mathrm{mm}^2$ Havar foil ($2.6 \pm 0.2\,\mu$m thick) supported by a cross frame (98% transparency, defined as the ratio between useful and total areas) so as to minimise the probability for foil breakage and deformation due to the pressure gradient. Havar is a metal alloy and allows an easy grounding of the window to the main pyramidal structure, moreover its good heat dissipation allows the use with very intense beam on target. Being free of hydrogen, it also allows to minimise proton contamination from beam-induced scattering on the window. The entrance window acts as a cathode to the IC and can be easily replaced to meet the requirements of specific applications (*e.g.*, to sustain higher gas pressures in the IC or to minimise energy losses and to reduce thresholds for charged particles). The anode is a $52.5 \times 52.5\,\mathrm{mm}^2$ Mylar foil ($1.5 \pm 0.2\,\mu$m thick), metallised with $50\,\mu\mathrm{g/cm}^2$ of aluminium and mounted 116 mm behind the entrance window. The distance cathode-anode therefore defines the active region of the IC. The Frisch grid consists in a mesh of gold-coated tungsten wires ($20\,\mu$m diameter) arranged perpendicularly to one another at 3 mm pitch in both directions ($\simeq$ 99% transparency). The grid is placed upstream of the anode at a distance of 9.5 mm and is kept at a positive voltage lower than that used for the anode. The bias applied to the Frisch grid reduces to zero (ground) at the cathode through a resistive partition of guard rings connected in series by means of 3.3 MΩ resistors, as shown in fig. 3. Each guard ring consists in a gold-coated copper strip (3 mm width, 4 mm pitch) printed on the inner face of each side of the fiberglass pyramid. Special care was taken to avoid any deformation of the electric field inside the IC's active region, by minimising discontinuities arising from the soldering of metallic parts (guard rings and Frisch grid wires).

For the ^{12}C experiment, the IC was operated with CF_4 gas. The choice of this gas was favoured to, for example, isobutane because of its higher electron drift velocity, its higher ionisation power and its hydrogen-free composition, an important feature to minimise any source of proton background in the $^{12}\mathrm{C}(^{12}\mathrm{C},\mathrm{p})^{23}\mathrm{Na}$ cross-section measurements. The CF_4 enters the IC active region close to the entrance window guided by a Rilsan [19] pipe (external and internal diameters of 4 and 2 mm, respectively) from the gas inlet connector at the back of the housing. It flows out through the outlet connector also placed at the back of the aluminium housing. Typical values for the gas flow for a single IC were in the range 0.1–1 litres/h and are measured by a MKS PR4000B flow-meter. The pressure inside the IC is set and maintained constant, within ± 0.25 mbar, using an automatic system based on a MKS 250E pressure controller. The aluminium housing is sealed for in-vacuum operations and acts as gas container with a volume of about $1.5\,\mathrm{dm}^3$. Being electrically grounded, it also shields the IC electrodes and the inner readout electronics from the environmental electromagnetic noise.

3.2 Silicon strip detectors

The second stage of GASTLY consists in a large (active area of about $58 \times 58\,\mathrm{mm}^2$, $300 \pm 15\,\mu\mathrm{m}$ thick) silicon strip detector (SSD, mod. PF-16CT-58*58-300EB/D4) by CANBERRA Ltd. [20]. Its front face is segmented in 16 strips ($3.5 \times 58.0\,\mathrm{mm}^2$ each) separated by about 0.1 mm of passivated inter-strip region, while the conductive back plane is unsegmented. The detector's dead layers, according to specifications, are less than 50 nm on the front side and less than 1500 nm on the rear one. The SSD is completely depleted at an operating bias of 40 V and individual strip connections are provided through a Kapton flat cable terminated with a DB25 connector. The detector capacitance is $C_\mathrm{d} \simeq 1000\,\mathrm{pF}$ for the unsegmented pad, but about an order of magnitude lower for individual strips.

The opening size of the pyramid was chosen to maximise the solid angle covered by the silicon detector placed immediately behind the IC. The SSD is mounted 11 mm behind the IC anode, *i.e.* at an overall distance of $181\,\mathrm{mm} = (54 + 116 + 11)\,\mathrm{mm}$ from the target centre, thus subtending a solid angle of about 103 msr. Because of mechanical constraints, the SSDs centered at 156.5° were placed at an overall distance of 201 mm from the target and their nominal solid angle is also sensibly reduced by the shadow of the IC electrodes on the SSD (about 50 msr). To correctly evaluate the GASTLY module efficiency it is very important to consider, beside the solid angle coverage, also the entrance window cross frame transparency and the Frisch grid one (98% and 99%, respectively). Also the intrinsic efficiency of the SSD should be taken into account, especially when an individual strip readout system is used and very low-energy particles detected. A dependence of the effective inter-strip width (EIW) by the detector bias voltage, by the particle penetration depth and, in general, by the detector manufacturing features has been evidenced [21] and should be considered. In the present GASTLY set-up, where the SSD energy signals are read-out from the detector unsegmented back side (all strips being short circuited), only the SSD energy resolution results affected by this effect. A good practice, before each experiment, is to compare the efficiency calculation with an efficiency measurement performed with α-particle source placed at the target position and with an elastic scattering measurement on a well known target.

3.3 Electronics and readout

In order to minimize any source of electronic and environmental noise, that would adversely affect detection of low-energy particles, the GASTLY readout electronics is mounted on printed circuit boards arranged in a stack behind the SSD and inside the aluminium housing. A picture of the fully assembled detector with its readout electronics without and with the outer aluminium housing is shown in the left-hand and right-hand panels of fig. 4, respectively.

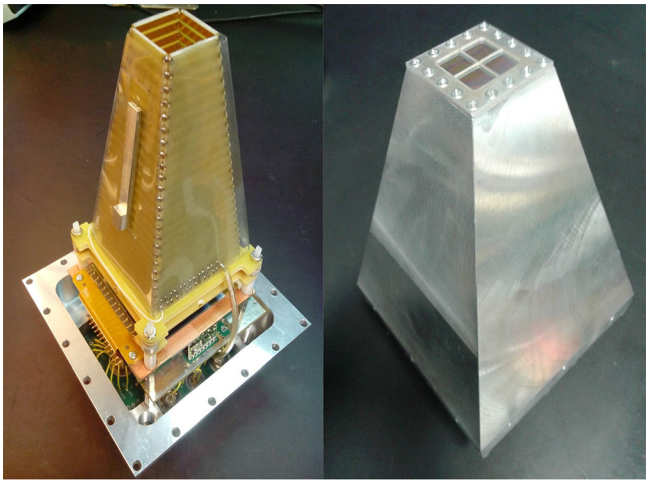

Fig. 4. Picture of the IC assembled components and readout electronics (left) and external aluminium housing (right).

Table 2. CHAPLIN specifications.

Input capacitance:	30 pF
Risetime @ Csource = 2 pF:	22 ns
Falltime @ Csource = 2 pF:	3.3 μs
Measured sensitivity:	30 mV/MeV in silicon eq.
Noise @ Csource = 0 pF:	300 e rms
Feedback capacitance:	1 pF
Feedback resistance:	10 MΩ
Open loop gain:	10^4 V/V
Power dissipation:	180 mW
Max energy converted:	200 MeV (+ve output signal)
	270 MeV (−ve output signal)
Output signal polarity:	inverted
Power supply:	+12 V, −12 V

The boards contain the IC bias filtering circuit (shown schematically in fig. 3), the temperature (AD22100KTZ) and pressure (SSCSANN015PAAA5) sensors, and the readout electronics. The readout electronics consisted in two home-made hybrid low-noise charge preamplifiers, CHAPLIN (CHArge Preamplifier Low-noise Infn Naples), one for the SSD signal and one for the IC anode signal. These preamplifiers have been widely used in the past with different experimental devices, showing excellent performance [22–24]. Their main features are summarised in table 2. The CHAPLIN output signals are fed into a 16-channel shaping spectroscopy amplifier, SPAM (SPectroscopy AMplifier), designed to match the CHAPLIN low-impedance output. The main features of SPAM are summarised in table 3. Note, however, that initial campaigns for the ^{12}C experiment were performed without individual strip readout.

Feedthrough connectors for pressure and temperature readout, SSD and IC output signals, pulser test input,

Table 3. SPAM specifications.

Input:	16 ch. (50 Ω or 1 kΩ) (coax. cable)
Output:	16 ch. (max gain 1000×) (IDC conn.)
X-output:	16 ch. (max gain 10000×) (IDC conn.)
Fast-output:	16 ch. (IDC conn.)
Output standard:	differential or single ended
Fine gain:	12 bit DAC (via software)
Coarse gain:	3 bit DAC (via software)
Shaping time:	0.5, 1.0, 2.0 and 4.0 μs (via software)
P-Z cancell.:	12 bit DAC full scale (via software)
Output pol.:	positive or negative (via software)
Fast-out pol.:	positive or negative (via software)
Fast-out gain:	1× or 5× (via software)
Base-line restor.:	automatic
Power dissip.:	42 W (+12 V [1.6 A], −12 V [1.5 A], +6 V [0.6 A], −6 V [0.2 A])

low-voltage bias for the readout electronics and high-voltage biases for the SSD, IC anode and grid, were mounted on the rear panel of the Al housing. All connectors were provided by FISCHER Connectors srl (model series 101, 103, 104 and 105) and allowed for operation under vacuum at 10^{-6} mbar.

4 Detector tests and performance

Initial tests on the performance of GASTLY were carried out on a prototype module at the Laboratorio di Astrofisica Nucleare of the Università degli Studi di Napoli Federico II, using α-particles from a mixed α-source (^{239}Pu, ^{241}Am and ^{244}Cm) with energies of 5.158, 5.487 and 5.806 MeV, respectively.

The IC is properly working when the whole charge released by a particle passing through the active region is collected at the IC electrodes. The charge collection efficiency is directly proportional to the reduced electric field, E/P, between the IC electrodes, with E and P the electric field and gas pressure, respectively. If the charge is completely collected, a further increase in the reduced electric field E/P does not produce amplitude variations of the anode signal, and thus of the peak position in the particle energy spectrum. Typically, the reduced electric field between the Frisch grid and anode $(E/P)_{\rm GA}$ is kept at a higher value than that between the cathode and Frisch grid $(E/P)_{\rm CG}$, but the effect of varying their ratio, within a factor of 3–6, on the signal amplitude and on its rise time was found to be negligible.

We measured the peak position in the energy spectrum of the α-particles, while varying $(E/P)_{\rm CG}$ in the range 0.3–1.4 kV/(cm atm) and $(E/P)_{\rm GA}$ in the range 1.2–4.0 kV/(cm atm) and found an improvement of $\leq 4\%$ in charge collection, due to the reduction of the border

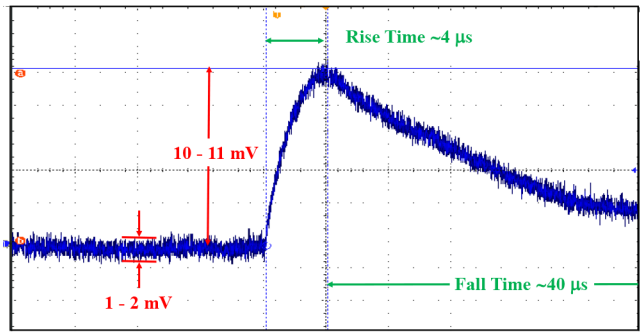

Fig. 5. CHAPLIN preamplifier output signal corresponding to an energy of about 3 MeV released by an α-particle inside the IC of a GASTLY module. Amplitude, rise and fall time of the signal and the peak-to-peak noise are indicated.

effects for particles with paths nearest the IC walls. This confirms that the IC worked properly in the ranges indicated above. Different E/P values were obtained by varying the electrode potentials up to 1.2 kV and the operating pressure up to 300 mbar (using a Havar window). No gas leakage was observed at these pressures and a breaking point for the Havar window was reached only at a pressure of about 800 mbar.

Figure 5 shows a sample preamplifier output signal produced by an α-particle depositing about 3 MeV in the active region of the IC. The amplitude of the signal is about 10–11 mV, with a rise-time and fall-time of about 4 μs and 40 μs, respectively. Typical noise peak-to-peak values are about 1–2 mV, which implies that low-energy particles ($\leq$ 1 MeV) will produce signals with a high enough signal-to-noise ratio already at the pre-amplification stage. Further signal processing was done using purpose-built main amplifiers (see sect. 3.3).

The energy resolution of the IC was determined using CF_4 gas at $P = 200$ mbar to completely stop the α-particles in the IC active region. The corresponding $E_{\rm IC}$ spectrum is shown in fig. 6, for the values of the reduced fields indicated. The energies corresponding to the peak centroids and their FWHMs are also quoted. The energy loss of α-particles in the entrance Havar window, as well as in the other dead layers and in the gas, was calculated using SRIM [25] code (and checked with LISE++ [26]) for the measured thicknesses of 2.6 μm and 1.5 μm for the Havar and the Mylar foils, respectively. The FWHM values correspond to an overall resolution for the IC of about 3% at the energies considered, and it does not change for gas pressure up to 350 mbar and also in the operational range 30–70 mbar as shown in fig. 7 for α-particles from a three-peak source and therefore in the relevant energy range 950 keV $< E_{\rm IC} <$ 3000 keV. The reduced fields E/P between cathode and Frisch grid and that between Frisch grid and anode were kept constant at the indicated values and the measured α-particle energies, determined taking into account energy losses, are given for the two extreme peaks. Typical resolutions of better than 2% (FWHM $\simeq$ 80 keV) were obtained for source α-particles stopped in the SSD without gas in the IC, but a worsening of

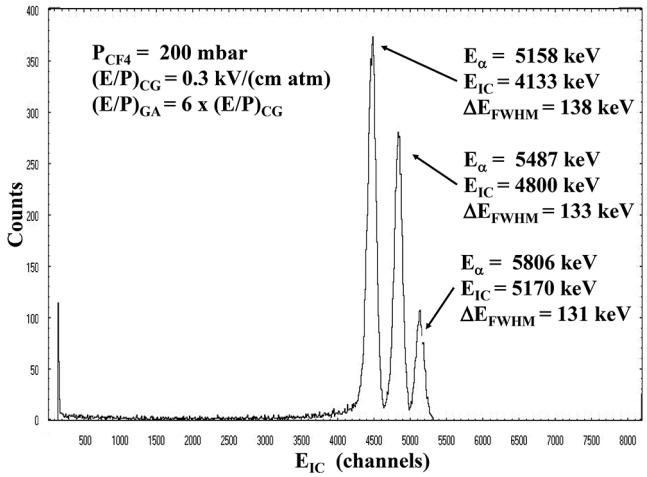

Fig. 6. $E_{\rm IC}$ spectrum for α-particles emitted by a three-peak source taken with IC fields and gas pressure values as indicated. Typical energy resolution for the IC was measured to be about 3%. (See text for $(E/P)_{\rm GA}$ and $(E/P)_{\rm CG}$ definition)

.

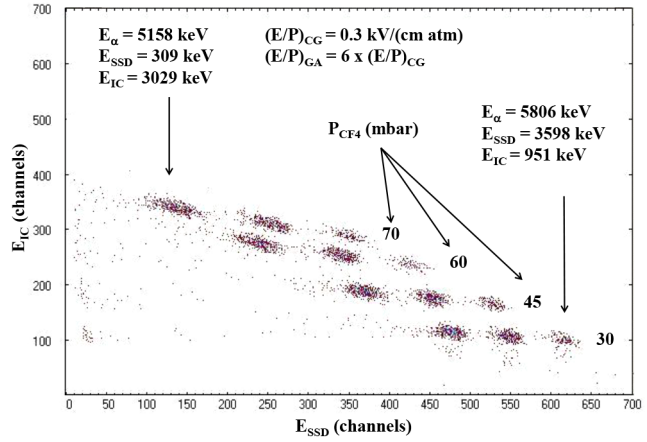

Fig. 7. $E_{\rm IC}$ *vs.* $E_{\rm SSD}$ matrix for α-particles emitted by a three-peak source obtained for different gas pressures in the IC. IC fields were maintained constant at the values indicated. Measured energies in both the ionisation chamber and the silicon strip detector are given for the two extreme α-particle peaks.

the overall SSD resolution, due to the α-particle energy straggling and to their energy loss in the gas, with the increasing of the pressure, can be observed (FWHM increases from 100 keV up to 200 keV and the energy lost in the SSD decreases from 3500 keV down to 300 keV, for a gas pressure ranging from 30 to 70 mbar) We also noted that an uncertainty of not less than 2–3% should be considered when energy loss calculation are performed with the cited codes in this energy region. The relative yields of each peak are comparable, albeit not exactly the same. As long as enough statistics are accumulated, the exact yield does not affect the energy resolution.

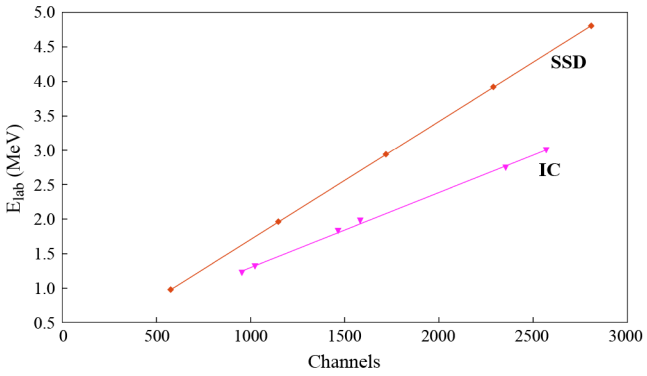

Fig. 8. Calibration of the SSD (obtained with protons of different energies elastically scattered by a thin gold target), and of the IC (obtained with a standard two-peak α-particle source at different gas pressures) for the detector placed at the $\theta = 156.5°$ UP position, corresponding to the position n. 7 of table 1.

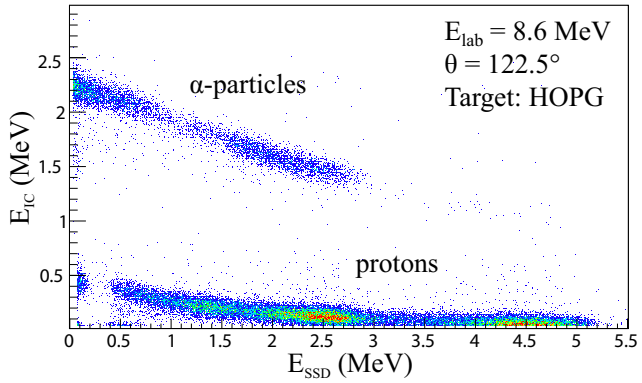

Fig. 9. $E_{\rm IC}$ *vs.* $E_{\rm SSD}$ matrix for the $^{12}{\rm C}+^{12}{\rm C}$ fusion reaction. Distinct loci corresponding to protons and α-particles from the $^{12}{\rm C}(^{12}{\rm C},{\rm p})^{23}{\rm Na}$ and $^{12}{\rm C}(^{12}{\rm C},\alpha)^{20}{\rm Ne}$ reactions, respectively, can be clearly identified.

4.1 In-beam tests with ^{12}C projectiles

To further characterise the performance of GASTLY, in-beam tests were performed at CIRCE, after proper calibration of the ICs and the SSD detectors. An example of calibration is reported in fig. 8, where the IC line was obtained using a two-peak α-particle source and different gas pressures, while, for the SSD, elastic scattering of a proton beam on a thin gold target at different energies was used. The linearity of the GASTLY electronics has been also tested with a pulser walkthrough in the range from zero to 10 MeV.

Figure 9 shows a typical ΔE-E matrix obtained with a GASTLY module placed at $\theta = 122.5°$ using a high intensity ($\simeq 20\,\mu$A) $^{12}{\rm C}^{3+}$ beam at $E_{\rm lab} = 8.6$ MeV impinging on an HOPG target (1 mm thick). Here, clear loci corresponding to protons and alpha-particles from the $^{12}{\rm C}(^{12}{\rm C},{\rm p})^{23}{\rm Na}$ and $^{12}{\rm C}(^{12}{\rm C},\alpha)^{20}{\rm Ne}$ reactions can be distinguished. The projection of the proton events onto the x-axis (fig. 10) shows that the energy resolution of the SSD is sufficient to distinguish different peaks $(p_0, p_1, \ldots)$ in the proton energy spectrum, corresponding to different

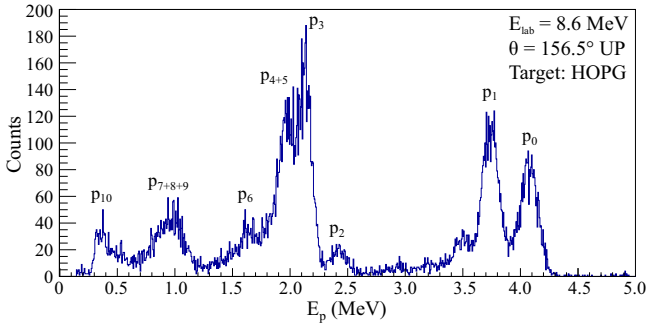

Fig. 10. Proton energy spectrum from the $^{12}C + {}^{12}C$ fusion reaction, obtained as x-projection of the proton locus in the E_{IC} *vs.* E_{SSD} matrix.

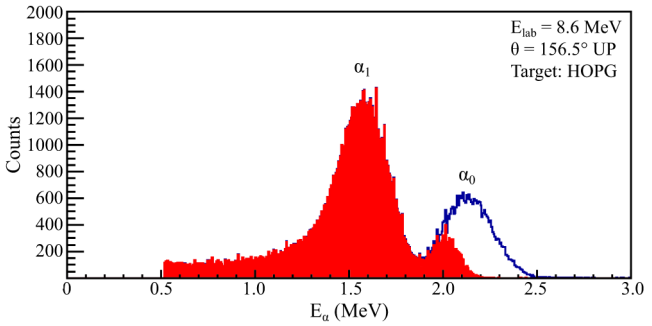

Fig. 11. Energy spectra of α-particles produced in the $^{12}C + {}^{12}C$ fusion reaction: in the red filled histogram only the α-particles completely stopped in the IC are reported; in the empty blue one, also the contribution of those stopped in the SSD is added ($E_\alpha = E_{IC} + E_{SSD}$).

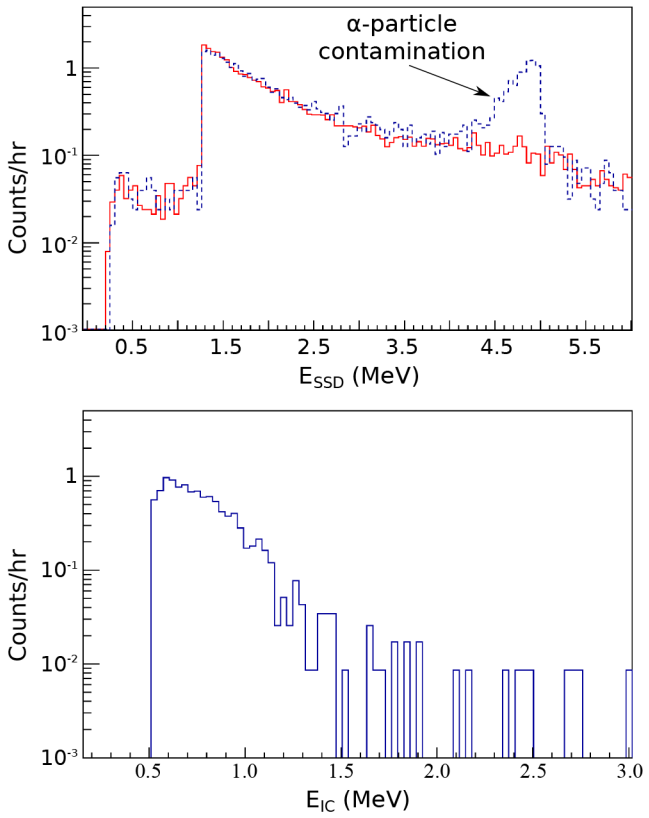

Fig. 12. Upper panel: energy spectrum of the intrinsic background in the SSD detector, showing an α-particle contamination peak (blue dashed histogram). The peak disappears (red continuous histogram) after covering the grid welding with a thin piece of paper. Lower panel: energy spectrum of the intrinsic background in the IC operated with 50 mbar of CF_4.

excitation states of the residual nucleus ^{23}Na populated by the reaction. The measured overall proton peak FWHMs of about 150–250 keV result from the combined effects of detector resolution, beam energy profile, target thickness effects, and (mostly) kinematic broadening due to the angular range covered by the detector.

The α-particle energy spectra shown in fig. 11 were obtained by taking into account the α-particles completely stopped in the IC without (red filled histogram) and with (blue empty histogram) the contribution of those passing through the IC and stopping in the SSD, whose energies were obtained by summing E_{IC} and E_{SSD}. Two peaks (α_0 and α_1) are visible, corresponding to transitions to the ground and first excited states of ^{20}Ne in the $^{12}C(^{12}C, \alpha)^{20}Ne$ reaction. The overall FWHMs are about 250–350 keV.

The intrinsic background of the GASTLY modules was determined through several-day long runs without beam or sources and revealed the presence of an unexpected wide peak at energies around 5 MeV in the SSD energy spectrum (blue dashed histogram, in the upper panel of fig. 12). This peak was identified as being due to α-particles emitted by contaminants in the metal alloy used for welding the grid wires; it disappeared (as shown in the red continous histogram, in the upper panel of fig. 12) after covering the grid welding with a piece of thin paper. The intrinsic background counting rate, over the full energy scale shown (region of interest for protons in the ^{12}C experiment), decreases from 2 counts/hr, at the lowest energies, to 4×10^{-2} at 6 MeV. At energies below 1.3 MeV only the contribution coming from the coincidence matrix is shown (about 3×10^{-2} counts/hr).

The intrinsic background of the GASTLY IC is shown in the lower panel of fig. 12. Its counting rate over the full energy scale shown (region of interest for the α-particles in the ^{12}C experiment) amounts to 1 counts/hr at 0.6 MeV and decreases to less than 10^{-2} at 2.5 MeV.

5 Individual strip read-out for angular distribution measurements

The GASTLY detection array offers the capability for angular distribution measurements through the read-out of individual strips of the SSD detectors. For this purpose, the Electronics Service of the INFN-Napoli, in collaboration with INFN-Catania, developed an ASIC chip (named MAGMA, Multichannel Analog front-end for seGMented silicon detector Application) in CMOS 0.35 μm technology, with 16 channels, each containing a charge preamplifier and a shaper circuit. Two different analog outputs

are available for each channel: a fast one (300 ns rise-time, negative polarity, conversion gain of 5.7 mV/MeV silicon equivalent and 0.8% linearity) for logic signal and trigger generation; and a slow one (1.5 μs rise-time, positive polarity, conversion gain of 7.5 mV/MeV silicon equivalent and 0.18% linearity). The chip has a large dynamic range (from 0 to $\pm$150 MeV in silicon equivalent) with a dissipation power of about 15 mW/channel which allows use in vacuum without cooling. The electronic noise for the slow output is very low (about 21 keV@0 pF with a slope of 107 eV/pF). During initial tests, the system was working at the lowest limit of its dynamic range and a further external amplification stage on the electronic board (based on common commercially available LM6172 and OPA37U operational amplifiers) was needed to increase the signal amplitude, which however introduced a higher electronic noise. The measured energy resolution of individual strips, for this reason, was comparable to that obtained for the unsegmented back-side of the detector. The angular resolution $\Delta\theta$, due to the width of the strips and to their rectangular shape, is of about 1.0°–1.5°.

A better energy resolution of the individual strip read-out, if necessary, could probably be achieved using a different electronic board equipped with 16 CHAPLIN preamplifiers (instead of the MAGMA chip board), but this requires that the associated high-power heating inside the detector housing be dissipated. This approach was discarded at present, but could be investigated in the future.

6 Conclusions and future directions

A new detection array, GASTLY, has been specifically designed for the detection and identification of light charged particles at low energies for nuclear astrophysics applications. The full array consists of eight ΔE-E modules comprising a ionisation chamber and a large area silicon strip detector. Tests performed with α-particle sources, as well as proton and ^{12}C ion beams, have confirmed the good energy and position resolution of the array and its suitability for the identification and measurement of low-energy charged particles and for angular distribution measurements.

The modularity of the GASTLY array also allows for use in different configurations and experimental set-ups. Characteristic spectra from initial studies of the ^{12}C + ^{12}C fusion reactions at energies below $E_{\rm cm} \simeq 4$ MeV at backward angles have been reported here, showing overall energy resolutions of about 3% for the ionisation chambers and of 2% for the silicon strip detectors.

Angular distribution measurement capabilities, although not exploited during the initial campaigns of the ^{12}C experiment, have also been demonstrated through the development of purpose-built read-out electronics based on a 16 channel ASIC chip technology.

Acknowledgements are due, for their help in the development of GASTLY, to the following people: L. Roscilli (Mechanical Design Service, INFN Napoli), F. Cassese, B. De Fazio and L. Panico (Mechanical Workshop, INFN Napoli). We are also indebted to V. Sipala (Università degli Studi di Sassari), N. Randazzo (INFN Catania) and S. Energico (CERN BE/RF-IS) for the development of the MAGMA chip.

References

1. C.E. Rolfs, W.S. Rodney, *Cauldrons in the Cosmos* (The University of Chicago Press, 1988).
2. C. Iliadis, *Nuclear Physics of Stars*, 2nd edition (Wiley-VCH, 2015).
3. G.F. Knoll, *Radiation Detection and Measurement*, 3rd edition (John Wiley & Son Inc., 2000).
4. W.R. Leo, *Techniques for Nuclear and Particle Physics Experiments* 2nd edition (Springer Verlag, 1994).
5. M.E. Bennett *et al.*, Mon. Not. R. Astron. Soc. **420**, 3047 (2012).
6. M. High, B. Ĉujec, Nucl. Phys. A **282**, 181 (1977).
7. K.U. Kettner *et al.*, Z. Phys. A **75**, 65 (1980).
8. P. Rosales, E. Aguilera, Rev. Mex. Fís. S **49(4)**, 88 (2003).
9. L. Barrón-Palos, E. Chavez, Rev. Mex. Fís. S **50**, 18 (2004).
10. L. Barrón-Palos *et al.*, Eur. Phys. J. A **25**, 645 (2005).
11. L. Barrón-Palos *et al.*, Nucl. Phys. A **779**, 318 (2006).
12. E. Aguilera *et al.*, Phys. Rev. C **73**, 064601 (2006).
13. T. Spillane *et al.*, Phys. Rev. Lett. **98**, 122501 (2007).
14. J. Patterson, H. Winkler, C. Zaidins, Astrophys. J. **157**, 367 (1969).
15. M. Mazarakis, W. Stephens, Phys. Rev. C **7**, 4 (1973).
16. H.W. Becker, K.U. Kettner, C. Rolfs, H.-P. Trautvetter, Z. Phys. A **312**, 305 (1981).
17. J. Zickefoose, ^{12}C+^{12}C *fusion: Measurement and advances toward the Gamow energy*, PhD Thesis, University of Connecticut, US (2010).
18. `https://www.instrumart.com/assets/Flir-SC325-Datasheet.pdf` (last accessed: July 22, 2018).
19. Rislan PA 11 by ARKEMA site, `https://www.extrememateriels-arkema.com/en/product-families/rilsan-polyamide-11-family/` (last accessed: August 22, 2018).
20. *PIPS Silicon Detectors Catalogue* Canberra Industries Inc., Meriden (USA), `http://www.canberra.com/products/detectors/pips-detectors-single-multiple.asp` (last accessed: July 22, 2018).
21. L. Grassi *et al.*, Nucl. Instrum. Methods A **767**, 99 (2014).
22. M. Romoli *et al.*, *Ann. Rep. INFN Legnaro 2005*, INFN-LNL-210 (2006) p. 178.
23. M. Romoli *et al.*, Eur. Phys. J. A **25**, 289 (2005).
24. M. Romoli *et al.*, IEEE Trans. Nucl. Sci. **52**, 1860 (2005).
25. J. Ziegler, *SRIM, The Stopping and Range of Ions in Matter* (2013) `http://srim.org` (last accessed: July 22, 2018).
26. O.B. Tarasov, D. Bazin, Nucl. Instrum. Methods B **376**, 185 (2016) `http://lise.nscl.msu.edu/lise.html`.